

Hyperfine interaction in the lowest levels of the 3H_4 and 1D_2 states of trivalent praseodymium in yttrium aluminum perovskite ($YAlO_3$)

L. E. Erickson

National Research Council, Ottawa, Canada K1A 0R6

(Received 6 December 1978)

The hyperfine interaction in the lowest levels of the 3H_4 and 1D_2 states of praseodymium in yttrium aluminum perovskite has been measured. The ground-state (3H_4) measurements were made using a rf optical technique. The excited-state (1D_2) measurements were made using an enhanced and saturated absorption method. The energy-level separations, spin-Hamiltonian parameters, ground-state magnetic splitting factor and orientation, and the ground-state linewidths are reported. The crystal-field splittings of the 3H_4 and 1D_2 manifolds were measured.

I. INTRODUCTION

Heteronuclear and hyperfine interactions play important roles in the optical spectra of guest ions in optical crystals. The linewidths of the no-phonon lines of these guest ions at low temperatures are largely determined by the interactions with the host nuclei.¹ It follows that a narrower optical linewidth should be observed for a given ion in a host with smaller nuclear dipole moments. Also the hyperfine interaction, which is large enough to yield level splittings greater than the linewidth in the $LaF_3:Pr^{3+}$ system, produces a large modulation of the photon-echo amplitude as the pulse separation is increased.² The comparison of this modulation with that predicted from the hyperfine splittings is made difficult because the total upper-state energy-level separation is nearly equal to one of the ground-state separations, and because the large discrete pulse separations inherent in an optical delay-line experiment do not give sufficient resolution to follow the intricate modulation pattern. In this paper, I present a study of the hyperfine interaction in the ground electronic level (3H_4) and in the lowest level of the 1D_2 manifold of states for the praseodymium ion in yttrium aluminum perovskite ($YAlO_3$) otherwise known as yttrium orthoaluminate. The largest and only significant contributor to the heteronuclear interaction is the aluminum nucleus which produces a magnetic intensity at the praseodymium nuclei of 1 oersted full width at half maximum (FWHM). This compares to a magnetic intensity at the praseodymium nucleus of 3.8 oersted (FWHM) produced by the fluorine nuclei in lanthanum trifluoride. This should lead to a significantly narrower optical linewidth for $YAlO_3:Pr$ than for

$LaF_3:Pr$. The point symmetry of the praseodymium ion is C_{1h} in $YAlO_3$ compared to C_{2v} in LaF_3 . The no 3H_4 - 1D_2 phonon line in $YAlO_3$ is not symmetry forbidden as it is in LaF_3 , which means the optical absorption in $YAlO_3$ is much stronger than for LaF_3 . Therefore, the photon-echo measurements of praseodymium in $YAlO_3$ may be made with the gated cw-laser technique which gives complete control of the pulse separation and also significantly improved laser linewidths compared to the pulsed-laser techniques usually employed. It should be possible therefore to resolve the question of the significance of the laser linewidth on the photon-echo amplitudes.

II. OPTICAL SPECTRA

The magnitude of the hyperfine interaction is a function of the electronic energy-level splittings through a second-order magnetic hyperfine interaction. Any meaningful analysis of the hyperfine measurements therefore requires knowledge of the optical spectra. Many rare-earth ions have been studied in the yttrium aluminum perovskite single-crystal host.³ However, no optical measurements of the crystalline electric-field splittings of the praseodymium ion in this host have been reported. The crystal structure has been carefully studied.⁴ It has an orthorhombic unit cell, and a space group $D_{2h}^{16}-Pbnm$. The two inequivalent yttrium ions are at sites of point symmetry C_{1h} . An alternative choice of axes has been given by Diehl and Brand,⁴ however this paper will use the axis labels given by Geller and Wood.⁴ The praseodymium ion enters the lattice substitutionally for yttrium with no charge compensa-

TABLE I. Character table for C_{1h} symmetry with the transformation properties of the coordinates and angular momentum shown.^a

	E	σ_h	Transformation Properties	
Γ_1	1	1	x, y, J_z	x^2, y^2, z^2, xy
Γ_2	1	-1	z, J_x, J_y	xz, yz

Polarization of the optical transitions (electric dipole).^b

	Γ_1	Γ_2
Γ_1	σ	π
Γ_2	π	σ

^aSee Ref. 7.

^bSee Ref. 6.

tion necessary and therefore also has a point symmetry C_{1h} . This low symmetry crystalline electric field produces $2J + 1$ nondegenerate levels for each manifold of states. For ions in this symmetry all optical transitions are allowed and are polarized.

Optical measurements were made in absorption at low temperature (5–10 °K) to study the 1D_2 energy levels. As will become apparent, only the ground level of 3H_4 has a significant population at these temperatures. Measurements were also made in emission using selective laser excitation of the luminescing level in the same temperature range to determine the 3H_4 crystal-field split energy levels. Both sets of measurements were made using a 1-meter Czerny-Turner monochromator of resolution ~ 0.1 Å. The oriented (0.05 at. %) praseodymium-doped yttrium perovskite single crystal was purchased from the Atomergic Chemical Company. Previous studies¹ of praseodymium in lanthanum trifluoride have shown that the optical and magnetic resonance measurements are free from guest-guest interactions at concentrations of 1 at. % or less¹ so that only a single-ion optical spectrum should be observed. The results of these measurements are summarized in Fig. 1. Two characteristics should be noted: (i) the energy levels are more widely spaced than for $\text{LaF}_3:\text{Pr}^{3+}$, and (ii) a completely polarized spectrum is observed as expected for this point symmetry.⁶ The polarizations shown refer to luminescence transitions from the lowest 1D_2 level to the 3H_4 levels, and to absorption transitions from the ground level (3H_4) for the 1D_2 levels. The point symmetry properties determine the electronic wave functions, and completely determine the polari-

zation of the electronic transitions. The character table for C_{1h} symmetry is reproduced in Table I.⁷ From this table and the transformation properties of x, y, z coordinates, the polarization for electric dipole transitions can be written down as shown in Table I.⁶ The wave functions must also transform like the character of the irreducible representation of C_{1h} . The symmetry adapted wave functions are given in an elegant treatment reviewed by Bradley and Cracknell.⁸ For even J , they may be written down

$$|J, \Gamma_1\rangle = \sum_{J_z \text{ even}} a_{J_z}^f |J, J_z\rangle$$

and

$$|J, \Gamma_2\rangle = \sum_{J_z \text{ odd}} a_{J_z}^g |J, J_z\rangle$$

Now by simply counting the levels in Fig. 1, it is concluded that the lowest levels of 3H_4 and 1D_2 are Γ_1 . Therefore, the σ, π labels should be replaced $\sigma \equiv \Gamma_1, \pi \equiv \Gamma_2$. Absorption measurements at 77 °K where the 3H_4 (51 cm^{-1}) level is also populated confirm this assignment. No unexpected levels are observed (i.e., there are no symmetry forbidden transi-

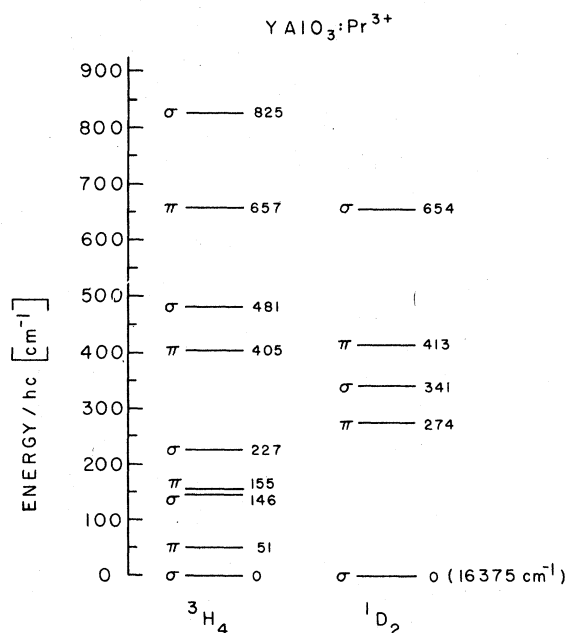


FIG. 1. Measured energy levels of the lowest crystal-field manifold of states 3H_4 , and the 1D_2 manifold of states. The levels are labeled by the polarization of the fluorescence from the lowest 1D_2 state to the 3H_4 state, and the polarization of absorption from the lowest 3H_4 state to the 1D_2 state. These labels are equivalent in this situation to the symmetry classifications $\sigma \rightarrow \Gamma_1, \pi \rightarrow \Gamma_2$ for C_{1h} site symmetry.

tions). Unfortunately, in this low symmetry it is not easy with this small amount of data to obtain further information about the wave functions via a crystal-field fitting procedure. This limits the analysis in the hyperfine interaction studies to upper bound situations.

The low-temperature linewidth in the non-phonon transition, ${}^1D_2(0) \rightarrow {}^3H_4(0)$, can be estimated if the emission linewidth of ${}^1D_2(0) \rightarrow {}^3H_4(51 \text{ cm}^{-1})$ is known⁹ because all of the other energy levels in these manifolds of states are much more widely separated from the lowest levels. The linewidth was measured by exciting the ${}^1D_2(0)$ level with a single mode stable dye laser and by observing this emission width with a Fabry-Perot interferometer. The observed width was 2.5 GHz at 8°K. This gives only an upper bound to the direct phonon line broadening because of the residual inhomogeneous broadening evident in non-resonant fluorescence-line-narrowing experiments.¹⁰ This is expressed as $\Delta\nu \leq 2.5P(51 \text{ cm}^{-1})$ GHz where

$$P(\Delta E) = [\exp(-kT/\Delta E) - 1]^{-1}$$

or at 5°K $\Delta\nu \leq 1 \text{ kHz}$! This is tempered slightly because the radiative lifetime which was measured to be 185 μsec for this 0.05% sample at 8°K contributes 1.7 kHz. At temperatures at or below 5 K, the phonon contribution to the optical linewidth is less than that from the radiative lifetime of the 1D_2 state. There will be no significant contribution from the phonons to coherence dephasing at these temperatures. Similarly, the absorption linewidth of ${}^3H_4 \rightarrow {}^1D_2(274 \text{ cm}^{-1})$ gives a measure of the ${}^1D_2(0)$ direct process width. The results are

$$\Delta\nu \leq 166P(274 \text{ cm}^{-1}) \text{ GHz} ,$$

or 23 kHz at 25°K and 10^{-27} Hz at 5°K, clearly negligible. While this is by no means a complete analysis of the optical spectra of $\text{YAlO}_3:\text{Pr}^{3+}$, the data are sufficient for an analysis of the hyperfine interaction reported in this paper.

III. GROUND-STATE (3H_4) HYPERFINE STRUCTURE

The hyperfine structure of each single electronic level is composed of three doubly degenerate "nuclear" levels in the absence of an external static magnetic field. This zero-field splitting is caused by two experimentally indistinguishable interactions. The largest is the second-order magnetic hyperfine interaction; the other is the interaction between the nuclear quadrupole moment of the $I = \frac{5}{2}$ Pr nuclei and the electric-field asymmetry of the electrons in the ion and the crystalline electric field.^{11,12} The ground-state hyperfine splittings were measured by an optical

radio frequency technique which employs the large ground-state nuclear polarization which accompanies optical pumping in the no-phonon [${}^3H_4(0) \rightarrow {}^1D_2(16, 375)$] line to enhance the signal amplitude. The large nuclear polarization is reduced by inducing magnetic dipole transitions between the hyperfine levels and is detected by the large change in luminescence which accompanies this reduction in polarization. This method is so sensitive that the nuclear resonance of 10^{10} nuclear spins can be detected by observing the crystal luminescence with the unaided eye in a lighted room. It has been previously used for the $\text{LaF}_3:\text{Pr}$ system.¹

The crystal was excited by a 1–5-mW focused beam (12-cm focal length) of cw σ -polarized 6105.5 Å light at 5°K. A rf magnetic field was applied to the sample at an angle of $\frac{1}{4}\pi$ to the b crystal axis and perpendicular to the c crystal axis. The amplitude of the π -polarized luminescence from the ${}^1D_2(16, 375 \text{ cm}^{-1}) \rightarrow {}^3H_4(51 \text{ cm}^{-1})$ transition is observed as a function of the radio frequency. This is merely a monitor of the ground-state absorption and therefore the hyperfine level population. A typical result is shown in Fig. 2. Similar results were ob-

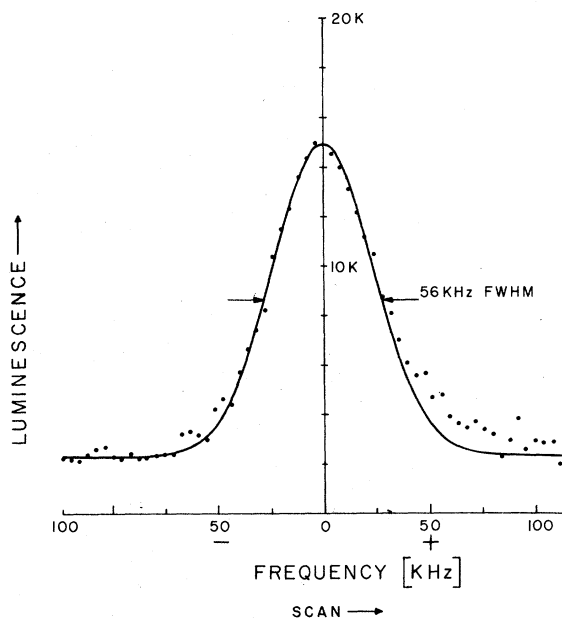


FIG. 2. Ground-state nuclear resonance absorption in the absence of an applied external magnetic field. The horizontal scale is centered at the peak of the nuclear resonance absorption. This zero frequency is 7.059 MHz. The rf magnetic field applied to the sample is approximately 0.008 G rms. The solid line is a Gaussian peak fit to the data. The poor fit on the right-hand side of the peak is due to sweep rate effects. This consists of four scans for which the sweep rate was 0.3 sec/channel.

served on monitoring the transmitted laser light. The rf magnetic field strength was about 8 mG rms. The solid line is a Gaussian curve fit to the data. The line shape is very closely Gaussian on the leading edge. The tail of the following edge, which lies above the Gaussian curve is due to the fast frequency sweep in these experiments. Each plotted point represents a dwell time of 0.3 sec and the frequency step between each is 3.99 kHz. The long nuclear spin-lattice relaxation times of the $\text{YAlO}_3\text{:Pr}$ crystal demand a slower sweep to avoid lineshape distortion. The measured linewidth, 56-kHz FWHM, however is not significantly affected by this distortion. Two resonant frequencies 7.057 ± 0.005 MHz and 14.100 ± 0.010 MHz were observed. These frequencies may be fit by a spin Hamiltonian

$$\mathcal{H} = D[I_z^2 - \frac{1}{3}I(I+1)] + (E/2)(I_+^2 + I_-^2),$$

where

$$|D| = 3.5255 \pm 0.0006 \text{ MHz}$$

and

$$|E| = 0.032 \pm 0.008 \text{ MHz}$$

The stated errors are the standard deviations obtained from the least-squares best fit of the Hamiltonian to the data.

From the analysis of this Hamiltonian given by Teplov,¹² we find that for $E=0$ that

$$\Lambda_{xx} = \Lambda_{yy}$$

where

$$\Lambda_{ii} = \sum_{n \neq 0} A_j \frac{|\langle 0 | J_i | n \rangle|^2}{E_n - E_0},$$

A_j is the hyperfine interaction constant, E_n is the energy of level $|n\rangle$, and z is the axis of quantization for the ion in the crystal field. It is reasonable to assume that the pure quadrupole interaction constant P is small compared to the observed hyperfine splitting constant D and because the first excited Γ_1 level lies at 146 cm^{-1} compared to the first excited Γ_2 level at 51 cm^{-1} , we can neglect the Λ_{zz} contribution to D . The "measured" value of $\Lambda_{xx} = \Lambda_{yy} = D/A_j = 0.0032$ from which we can calculate Teplov's magnetic splitting factor γ

$$\gamma_x = \gamma_y = g\beta\Lambda_{xx} = 1.3 - 18.0 = 16.7 \text{ kHz/G}$$

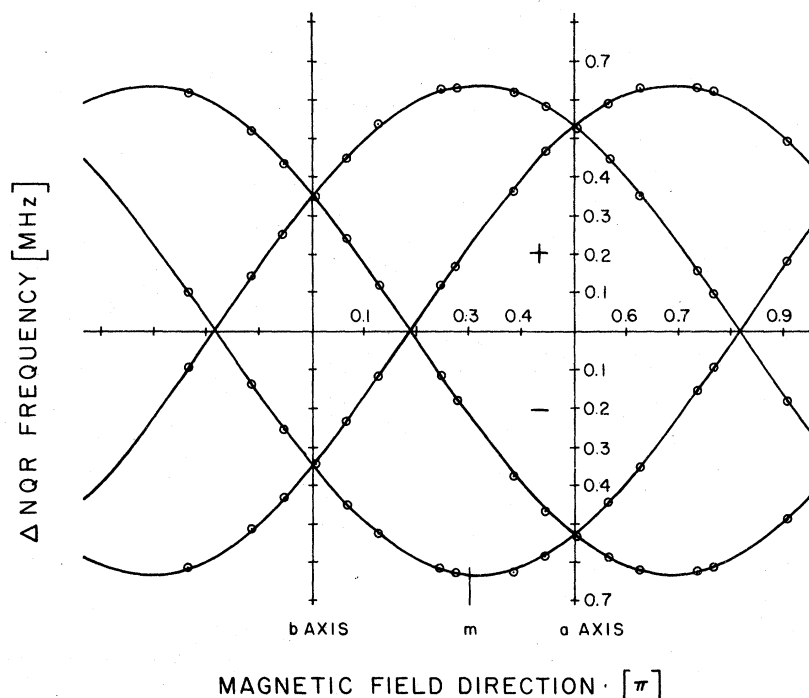


FIG. 3. The nuclear-quadrupole-resonance frequencies in an external static magnetic field of 54.21 ± 0.14 G. The field is always perpendicular to the c axis. The horizontal axis is the angle between the field and the crystal b axis. The maximum splitting obtained from the best fit cosine curve to the data (solid line) is 1.269 ± 0.002 MHz. The maximum splitting factor is 23.408 ± 0.078 kHz/G. The angle of the maximum splitting is $0.3139 \pm 0.0015\pi$ radians centered about the b axis and in the a - b plane. The diagram is marked with an m which is near the direction of maximum splitting for one of the two inequivalent sites for which data were taken in Fig. 4. The direction of maximum splitting is the nuclear z axis.

The maximum value of Λ_{xx} for a state separation of 51 cm^{-1} , obtained for a Γ_1 state $|0\rangle$, Γ_2 state $(1/2^{1/2})(|+1\rangle + |-1\rangle)$ choice of states is 0.0036 and for $\Gamma_1 = (1/2^{1/2})(|+2\rangle + |-2\rangle)$ is 0.0032. A ground state which is largely a mixture of $J_z = |0\rangle, |\pm 2\rangle$ would give the observed $\Lambda_{xx}, \Lambda_{yy}$. The maximum Λ_{zz} obtained for a $|J_z = \pm 2\rangle$ ground state is 0.0005. The upper bound for γ_z is $(1.3 - 2.8) = 1.5 \text{ kHz/G}$. The x, y, z axes are those of the ion in the crystal field. These must be transformed to those of the Pr nucleus before comparison with the experiment. It should be noted that at the low magnetic fields used in these experiments that the total magnetic field splitting is small compared to the zero-field splittings. The magnetic field terms $\gamma_z H_z + \gamma_x H_x + \gamma_y H_y$ are treated as a perturbation of zero-field wave functions. (The primes indicate the nuclear axes). The only first-order splitting is due to $\gamma_z H_z$, the second-order splittings due to γ_y, γ_x are much smaller. Thus the angular dependence of the resonant frequencies will be $\nu(H, \theta) = \nu_0 \pm \gamma_z H \cos\theta$. Since γ_z is near zero, the maximum possible γ_z' is calculated to be

$$\gamma_m = (\gamma_x^2 + \gamma_y^2)^{1/2} = 23.6 \text{ kHz/G}$$

The magnetic field splitting factor γ_z' and its direction was measured by a study of the nuclear resonance spectrum in a fixed magnitude, varying direction field of $54.21 \pm 0.14 \text{ G}$. A summary of the 14 MHz transition measurements is shown in Figs. 3 and 4. In these figures, the resonant frequencies for the two Pr^{3+} sites are plotted versus field angle with respect to the a, b, c crystal axes. Figure 3 shows the results when the field is in the $a-b$ plane. The maximum splitting for the two inequivalent sites occurs at angles of $\pm 0.3139 \pm 0.0015\pi$ radians from the b axis. For the field in the $m-c$ plane indicated in Fig. 3, the results are shown in Fig. 4. The maximum splitting occurs for the field lying along m (in the $a-b$ plane) and its complement for the second site. The maximum measured splitting factor is $\gamma_z' = 23.408 \pm 0.078 \text{ kHz/G}$. The calculated maximum splitting factor γ_m is in very good agreement with the measured value γ_z' .

The magnetic splitting factors γ_z' are the same for both sites, only the direction differs. The magnetic splitting for the field directed along the c axis is zero within experimental error of 5 kHz. The magnetic splitting should not be confused with γ_x' and γ_y' . If

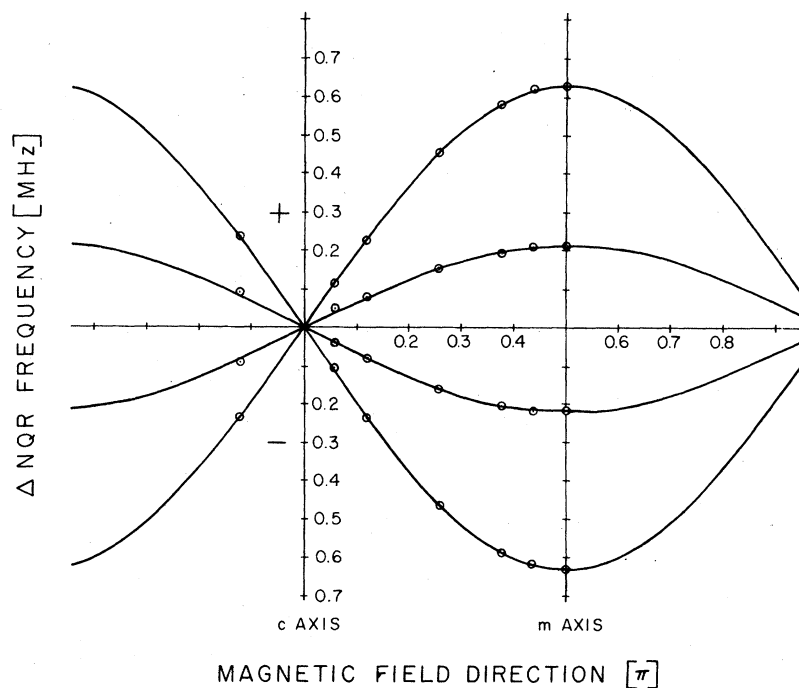


FIG. 4. The nuclear-quadrupole-resonance frequencies in an external magnetic field of $54.21 \pm 0.14 \text{ G}$ applied in the plane containing m and c . The horizontal scale measures the angle between the magnetic field vector and the crystal c axis. The m axis is near the direction of maximum splitting for one of the two nuclear sites. The measured deviation from this maximum direction is 0.013π radians which should lead to a 0.9990 multiplier for the maximum splitting. The best fit maximum splitting is $1.264 \pm 0.004 \text{ MHz}$ slightly smaller than the expected splitting but well within the statistical errors in the experiment. The best fit of the smaller splitting gives a measure of the angle between the two sites if the magnetic field is parallel to the larger nuclear spin. The calculated angle between the nuclear spins with a correction for field misalignment is $0.625\pi \pm 0.005\pi$ radians well within the statistical errors of the experiment.

$\gamma_s \approx 10$ kHz/G, a noticeable splitting of 5 kHz would occur in a 50 G field for a field angle $\theta = \frac{1}{2}\pi$. Studies of the 7 MHz transition were more complex because of the extra transitions which are present.¹³ The maximum magnetic field splittings for comparable $\Delta m_l = \pm 1$, transitions are identical for the 14 and 7 MHz transitions.

The linewidth is largely determined by the interaction of the nuclear spins of praseodymium with those of the aluminum. A calculation of the magnetic field at the praseodymium nucleus of the fourteen nearest-neighbor aluminum ($I = \frac{5}{2}$), for random populations of the Al nuclear substates gives a Gaussian field distribution for an ensemble of Pr^{3+} ions equal to 1.0 G FWHM. The "static" broadening of the resonance line is then 23 kHz FWHM. If more aluminum neighbors are included, a slight increase in the field strength is expected. The yttrium nuclei contributions which are omitted, are less than 0.1 G. The "dynamic" broadening which occurs because the magnetic field is modulated¹⁴ due to Al, Pr precession is calculated to be approximately 15 kHz. A third source of broadening, Pr^{3+} spin flips can be measured separately using a photon-echo or spin-echo technique. One other contribution to the resonance linewidth is the residual magnetic field 0.6 G, in this experiment a maximum of 14 kHz but field direction

dependent. These calculated values are approximately equal to the measured linewidth of 56 kHz. It is significant that the resonance lines have a Gaussian shape. If the major contributor to the line shape were a time limiting process such as spin flips, the line shape should be Lorentzian. The heteronuclear contribution should be largely Gaussian for the interaction of nuclear dipoles of similar sizes. This measurement demonstrates that the heteronuclear interaction is the major contributor to the resonance linewidth.

IV. EXCITED-STATE HYPERFINE STRUCTURE

The hyperfine splitting of the 1D_2 ($16,375\text{ cm}^{-1}$) state of $\text{YAlO}_3:\text{Pr}^{3+}$ is similar to that of the ground state $^3H_4(0)$ except that the second-order magnetic hyperfine interaction is much smaller. This is the result of a much larger energy-level splitting between the first and second 1D_2 states (274 cm^{-1}), and to the smaller J value. $P \ll D$ is no longer a good assumption. This study is only able to determine $|D|$, and $|E|$, can not separately obtain the D_a , E , P , and η parameters.

The hyperfine level separations of the 1D_2 ($16,375\text{ cm}^{-1}$) electronic state were measured using an

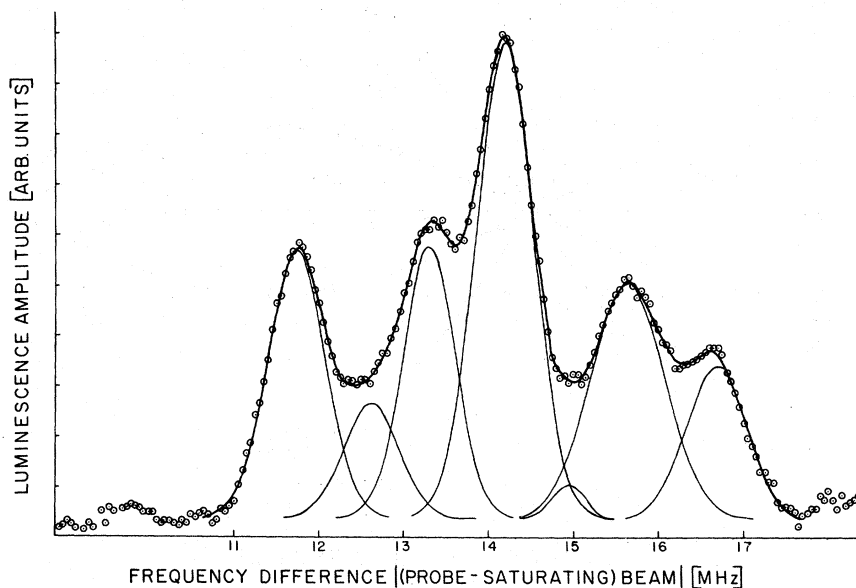


FIG. 5. Enhanced absorption spectrum near the 14 MHz ground-state energy-level separation at 5°K . The circles are the measurements of the luminescence amplitude vs the frequency difference between the optical saturating beam and the weaker optical probe beam. The upper solid line is the least squares best fit of the seven Gaussian components to the data. The lower solid lines are the individual components. The run consists of four 76 second sweeps in the presence of a 7 MHz rf magnetic field which enhances the signal strength. The baseline is at approximately 60 000 counts/channel. The major peak is approximately 100 000 counts. The laser linewidth FWHM is 250 kHz. The central peak best-fit linewidth is 603 kHz FWHM (Gaussian line shape).

enhanced absorption technique previously described.¹⁵ Briefly, the absorption spectra of the optically polarized nuclear substrates of the ground electronic state is probed optically with a monochromatic light source. The upper-state splittings are observed because the upper-state levels are coupled through a nonsymmetric hyperfine interaction. This leads to a nonzero transition probably connecting all upper states with all lower states. The enhanced absorption spectra consists of three groups centered about the ground-state splittings with various transition intensities. A maximum of seven lines may be observed in each group,

$$\begin{aligned} & \pm(\nu_1), \quad \pm(\nu_1 \pm \nu_2), \quad \pm(\nu_1 \pm \nu_3) , \\ & \pm[\nu_1 \pm (\nu_2 + \nu_3)] , \end{aligned}$$

where ν_1 is a ground-state splitting, and ν_2, ν_3 are the excited-state splittings to be determined. The $\pm\nu_1, \dots$ indicates that enhanced absorption occurs for the probe optical frequency both greater and less than the saturation optical frequency. In addition, seven saturated absorption lines may be observed at $0, \pm\nu_1, \pm\nu_2, \pm(\nu_1 + \nu_2)$. The sample was optically pumped with a 1-mW 6105.5-Å σ cw beam at 5°K, focused to a beam waist of $\sim 120 \mu$ diameter. The optical probe was generated by amplitude modulating the beam so that 0.01 to 0.05 of the power was in the sidebands. The laser linewidth was 250 kHz FWHM. As was noted previously,¹⁴ a radio frequency magnetic field, at a ground-state splitting applied to the crystal increases the signal to noise of the observed spectrum by increasing the population of the nuclear substate being studied.¹⁶ The enhanced absorption spectrum for the 14 MHz group is shown in Fig. 5. For this experiment, the modulation bias was adjust-

ed to give only the lower sideband plus carrier operation. The upper sideband power was less than 0.1, that of the lower sideband. The saturation and the probe transitions are interchanged with a sideband change. This leads to a different spectrum because of the differing intensity distributions. A rf magnetic field at 7.05 MHz of 0.3 G was applied to the sample to obtain the data shown in Fig. 5.

The spectrum consists of five clearly observable peaks. This spectrum was first fitted by five Gaussian shaped peaks but large deviations between the fitted curve and the experimental points were evident between the peaks at 11.7 and 13.2 MHz, and smaller deviations were evident near 15 MHz. The addition of two Gaussian shaped peaks gave a remarkably good fit to the observations. Attempts at Lorentz shaped fits were unsuccessful. The resultant parameters obtained from this least-squares fit are shown in Table II. Also given is the excited-state splittings obtained from this data only (Peak 5 was ignored).

The seven component peaks fulfill the maximum number of expected enhanced absorptions. The peak at 15 MHz has a linewidth one half of the others and an amplitude 0.13 of the adjacent main peak. This peak was ignored in the fitting procedures primarily because of its small linewidth (The frequency is near an expected absorption). All of the other peaks have a FWHM of about 780 kHz. The laser linewidth of 250 kHz FWHM contributes most of the observed linewidth, for it appears in the saturation beam (perhaps distorted to a larger linewidth) and in the probe beam. Since the form of the deconvolution is not known, the optical linewidth was not determined. It should be noted that the overall observed linewidth is about 100 kHz less than for the LaF₃:Pr³⁺ system with substantially the same apparatus. The dye nozzle

TABLE II. Least-squares fit parameters for the enhanced absorption spectra shown in Fig. 4. This is a fit of seven Gaussian peaks to the data. The errors are the standard deviations obtained from the fit. These data yield excited state splittings of $1.088 \pm 0.142, 1.485 \pm 0.170$ MHz with a central frequency of 14.226 ± 0.098 MHz.

Peak	Amplitude [arb. units]	Position [MHz]	Width (FWHM) [MHz]
1	26487 ± 391	11.677 ± 0.012	0.788 ± 0.018
2	11433 ± 1473	12.555 ± 0.065	0.751 ± 0.147
3	26779 ± 1744	13.247 ± 0.025	0.715 ± 0.059
4	47213 ± 288	14.147 ± 0.006	0.799 ± 0.020
5	3414 ± 904	14.905 ± 0.029	0.404 ± 0.084
6	23384 ± 217	15.609 ± 0.009	1.005 ± 0.052
7	15162 ± 428	16.636 ± 0.018	0.823 ± 0.029

zle is different resulting in a slightly increased laser linewidth in the present study.

The optical linewidth should be very nearly the same as that of the ground-state width. The magnetic field enhancement will be very small due to the large separation of the lowest 1D_2 electronic levels. The 1 G host magnetic field will therefore contribute only a few kHz. The lifetime of the 1D_2 state will contribute about 2 kHz maximum. The phonon contribution has been shown to be completely negligible at this temperature. These add at most 4 kHz to the ground-state linewidth. Clearly, further experiments with a much narrower linewidth laser would be useful to measure the optical linewidth.

It is obvious that all of the enhanced and saturated absorption data should be included in the determination of the energy-level separations. A summary of the observed frequencies, and the results of least squares best fit of the four energy-level separations to the data are given in Table III. A broad saturated absorption was noted near 1.1 MHz. This unresolved pair of lines at 1 and 1.4 MHz is not included in the table. Tables II and III should be considered together. The excited-state splitting obtained from the limited fit of Table II agree within the statistical significance of the fits. Since more data is used in Table III, the statistical significance is substantially improved. The common ground-state splitting also agrees within the statistical significance of the two data sets. All of the best fit frequencies are within four standard deviations of the measured values. The ground-state splittings obtained from Table III agree within statistical significance with those measured directly in Sec. III. These energy-level separations may be used to determine $|D|$ and $|E|$ parameters for the upper state,

$$|D| = 0.3899 \pm 0.0057 \text{ MHz}$$

$$|E| = 0.0824 \pm 0.0040 \text{ MHz}$$

In a similar analysis to that for the ground state we can show that a significant fraction of the measured D is due to the pure quadrupole interaction P . The lowest state of 1D_2 (Γ_1) is a mixture of $J_z = 0, \pm 2$. The second state ($\Gamma_2, 274 \text{ cm}^{-1}$) is a mixture of $J_z = \pm 1$. We can place an upper bound on Λ_{xx} by assuming

$$|\Gamma_1(0)\rangle = |0\rangle$$

$$|\Gamma_2(274)\rangle = \frac{1}{2^{1/2}} (|+1\rangle + |-1\rangle)$$

and remembering that A_J is different for the $J = 2$ state. One obtains $\Lambda_{xx} = 0.00015$. If we further assume $\Lambda_{xx} \approx \Lambda_{yy}$ and $\Lambda_{zz} \approx 0$, then $D_a = 0.12 \text{ MHz}$, about $\frac{1}{3}$ of the measured value of D . It is clear from this very crude estimate that the pure quadrupole contribution to D is very significant. The enhanced

magnetic field splitting factor is $\gamma_x \approx 1.3 - 0.8 = 0.5 \text{ kHz/G}$. The heteronuclear broadening of the upper state is of order 1 kHz or less.

Several additional experiments, such as a pure quadrupole resonance study of lanthanum-doped YAlO_3 and a crystal-field fitting to 1D_2 state would provide sufficient data to estimate the pure quadrupole con-

TABLE III. All frequencies obtained from enhanced absorption measurements and the best fit frequencies obtained from a multiple linear regression analysis.

	Measured	Best fit
1	23.750	23.700 ± 0.033
2	22.666	22.634 ± 0.035
3	22.140	22.238 ± 0.034
4	21.204	21.173 ± 0.023
5	20.140	20.108 ± 0.036
6	19.590	19.712 ± 0.034
7	18.715	18.647 ± 0.034
8	16.612	16.651 ± 0.034
9	15.603	15.586 ± 0.034
10	15.090	15.190 ± 0.036
11	14.136	14.124 ± 0.024
12	13.182	13.059 ± 0.034
13	12.588	12.663 ± 0.035
14	11.666	11.598 ± 0.033
15	9.535	9.576 ± 0.033
16	8.530	8.510 ± 0.036
17	8.040	8.114 ± 0.034
18	7.060	7.049 ± 0.025
19	5.555	5.588 ± 0.034
20	4.647	4.522 ± 0.035
21	2.519 ^a	2.527 ± 0.024

^a(saturated absorption)

Best-fit parameters for energy-level separations.

Excited state	Ground state
1.461 ± 0.025 MHz	14.124 ± 0.024 MHz
1.065 ± 0.026 MHz	7.0490 ± 0.025 MHz
	S = 0.0753

tributions to D . This experiment demonstrates that a very good measurement of the excited hyperfine splittings may be obtained using optically derived data obtained by the enhanced and saturated absorption technique. The statistical significance of the result is confirmed in the good agreement between the ground-state splittings measured by the enhanced absorption technique and by direct absorption as in Sec. III.

V. CONCLUSIONS

This study has looked at some of the important characteristics of the $\text{YAlO}_3\text{:Pr}^{3+}$ system. It is evident that $\text{YAlO}_3\text{:Pr}$ may play an important role in the study of the dynamic processes which occur in solids because of its experimentally favorable properties. They are (i) all electronic levels are single, (ii) the

6105.5-Å zero-phonon line absorption is strong in very dilute samples, (iii) the heteronuclear interactions are conveniently small and conveniently nonzero, (iv) guest rare-earth impurities which lead to troublesome ion-ion interactions are negligible because the host is not a rare earth, (v) excellent crystals are available commercially, and (vi) the large crystal-field splittings minimize second-order hyperfine interactions particularly in the excited state. $\text{YAlO}_3\text{:Pr}$ is by no means the ideal two-level system for coherence experiments but is substantially better than $\text{LaF}_3\text{:Pr}$ for most experiments.

ACKNOWLEDGMENTS

I wish to thank Craig Lindberg for some of the calculations, A. Szabo for many useful discussions, and E. Dimmock for technical assistance.

¹L. E. Erickson, *Opt. Commun.* **21**, 147 (1977).

²Y. C. Chen, K. P. Chiang, and S. R. Hartmann, *Opt. Commun.* **26**, 269 (1978).

³M. J. Weber, T. E. Varitimos and B. H. Matsinger, *Phys. Rev. B* **8**, 47 (1973).

⁴S. Geller and E. A. Wood, *Acta Crystallogr.* **9**, 563 (1956); R. Diehl and G. Brandt, *Mater. Res. Bull.* **10**, 85 (1975).

⁵The levels shown here near 410 and 655 cm^{-1} could be vibronic rather than electronic in origin. See M. J. Weber, *Phys. Rev. B* **4**, 3153 (1971); H. H. Caspers and H. E. Rast, *J. Lumin.* **10**, 347 (1975).

⁶G. H. Dieke, *Spectra of Energy Levels of Rare Earth Ions in Crystals* (Interscience, New York, 1968), p. 122.

⁷H. Eyring, J. Walter, and G. F. Kimball, *Quantum Chemistry* (Wiley, New York, 1974), p. 385, No. 12. $A' = \Gamma_1$, $A'' = \Gamma_2$.

⁸C. J. Bradley and A. P. Cracknell, *The Mathematical Theory of Symmetry in Solids* (Clarendon, Oxford, 1972), Chap. II.

⁹W. M. Yen, W. C. Scott, and A. L. Schawlow, *Phys. Rev.* **136**, A271 (1964).

¹⁰L. E. Erickson, *Phys. Rev. B* **11**, 77 (1975); T. Kushida and E. Takushi, *Phys. Rev. B* **12**, 824 (1975).

¹¹B. Bleaney, *Physica (Utrecht)* **69**, 317 (1973).

¹²M. A. Teplov, *Zh. Eksp. Teor. Fiz. [Soviet Phys. JETP]* **26**, 872 (1968).

¹³A. Abragam, *The principles of nuclear magnetism* (Oxford University, New York, 1961), p. 254.

¹⁴A. Abragam, *The principles of nuclear magnetism* (Oxford University, New York, 1961) p. 123, Eq. 55.

¹⁵L. E. Erickson, *Phys. Rev. B* **16**, 4731 (1977).

¹⁶This occurs because the differing ground-state spin-lattice relaxation times leave most of the population in the state which relaxes the slowest. Absorption from the other states is enhanced when the spin-lattice relaxation is paralleled with the magnetic-dipole transitions induced by this rf field.